Electronic Supporting Information to:

Fusion and Desulfurization Reactions of Thiomorpholinochlorins

Meenakshi Sharma, Subhadeep Banerjee, Matthias Zeller, Christian Brückner*

Department of Chemistry, University of Connecticut, Storrs, CT 06269-3060, U.S.A.

Department of Chemistry, Purdue University, 560 Oval Drive, West Lafayette, IN 47907-2084, United States.

** e-mail: c.bruckner@uconn.edu*

Table of Contents

[*meso*-Tetraphenyl-2,3-dimethylporphyrinato]Ni(II) (9Ni)

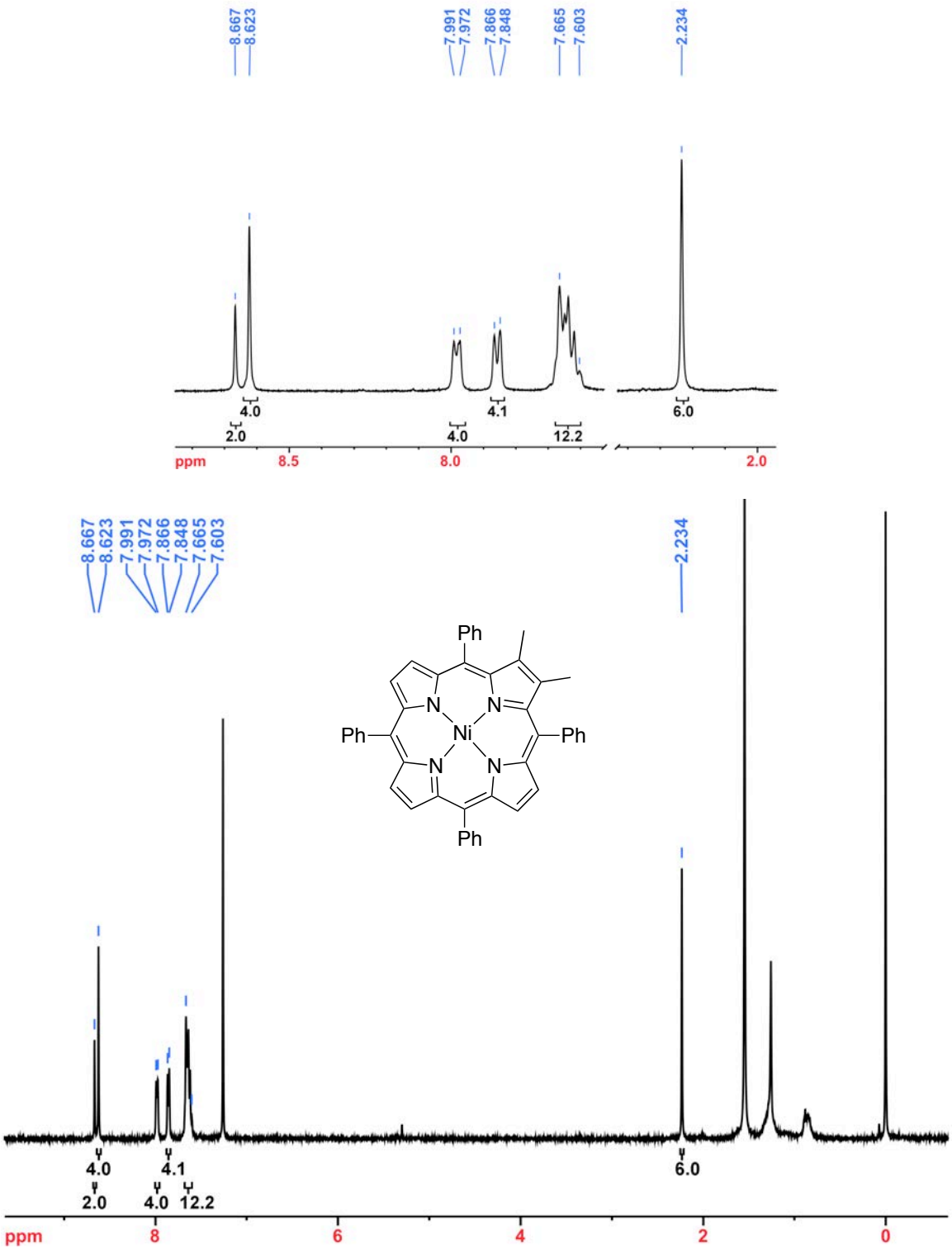

Figure S1. ^{1}H NMR spectrum (400 MHz, $CDCl_3$, 300 K) of **9Ni**

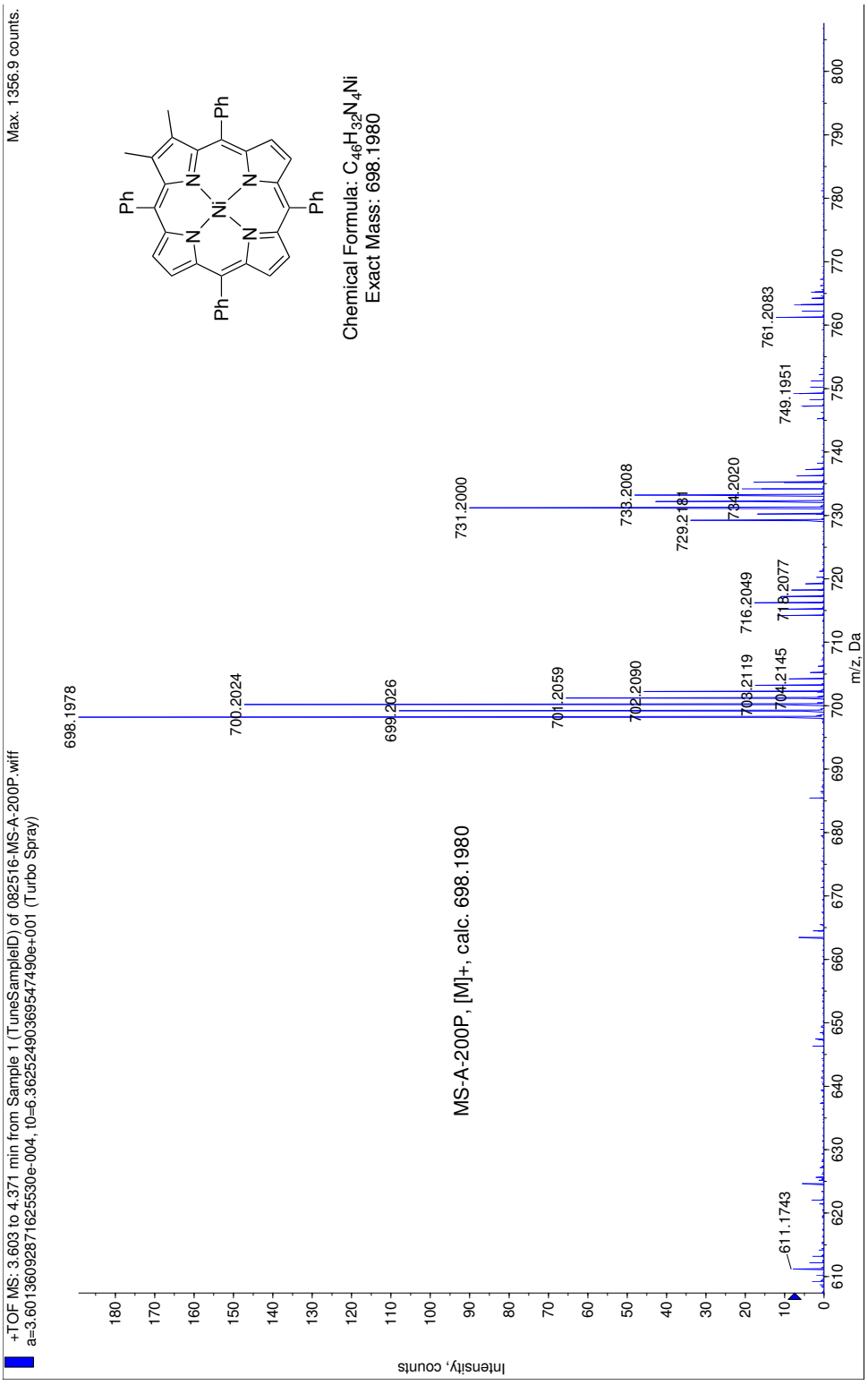

Figure S2. HR ESI+ MS (100% CH_3CN, TOF) of **9Ni**

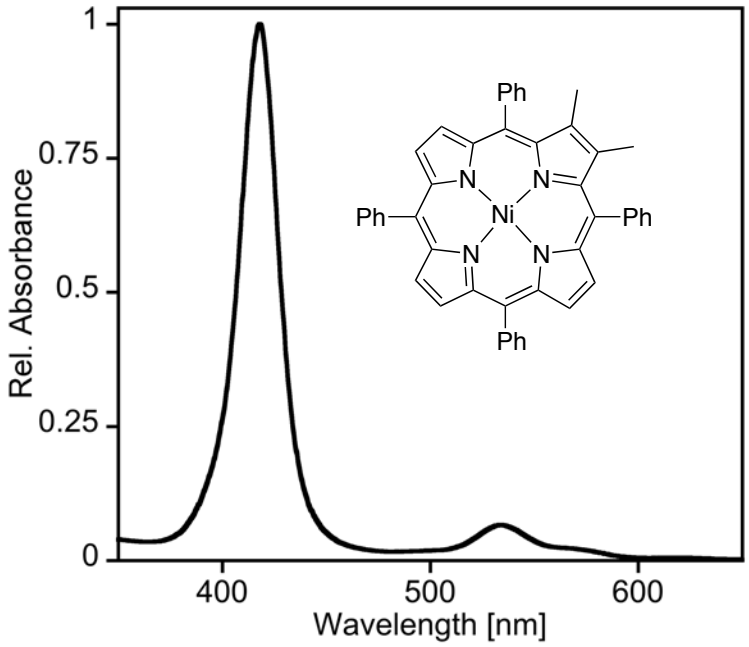

Figure S3. UV-vis spectrum (CH_2Cl_2) of **9Ni**

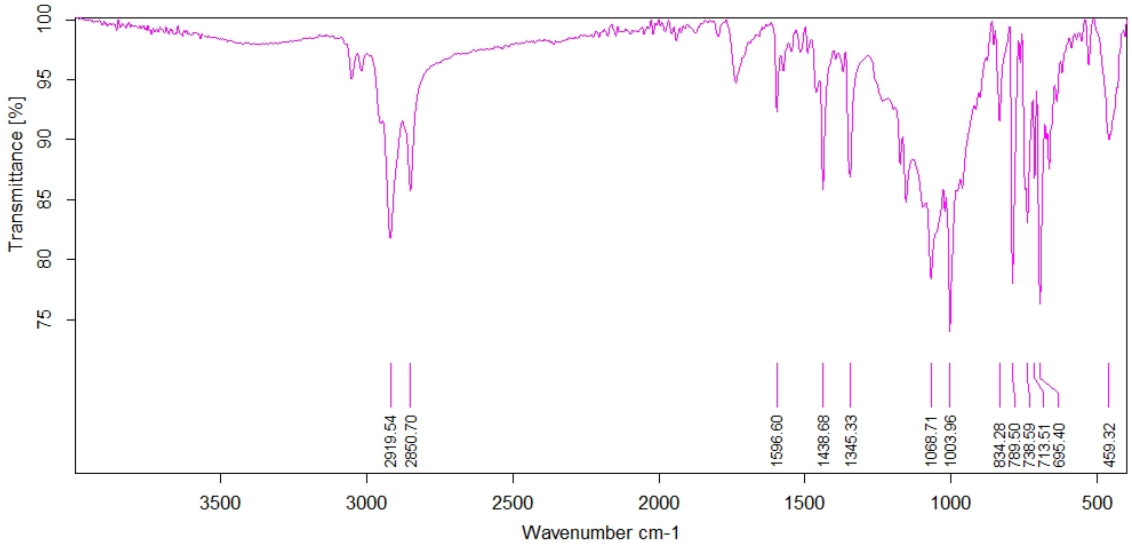

Figure S4. IR spectrum (neat, diamond ATR) of **9Ni**

[*meso*-Tetraphenyl-2,3-dimethyl-2*a*-thia-2*a*-homoporphyrinato]Ni(II) (10Ni)

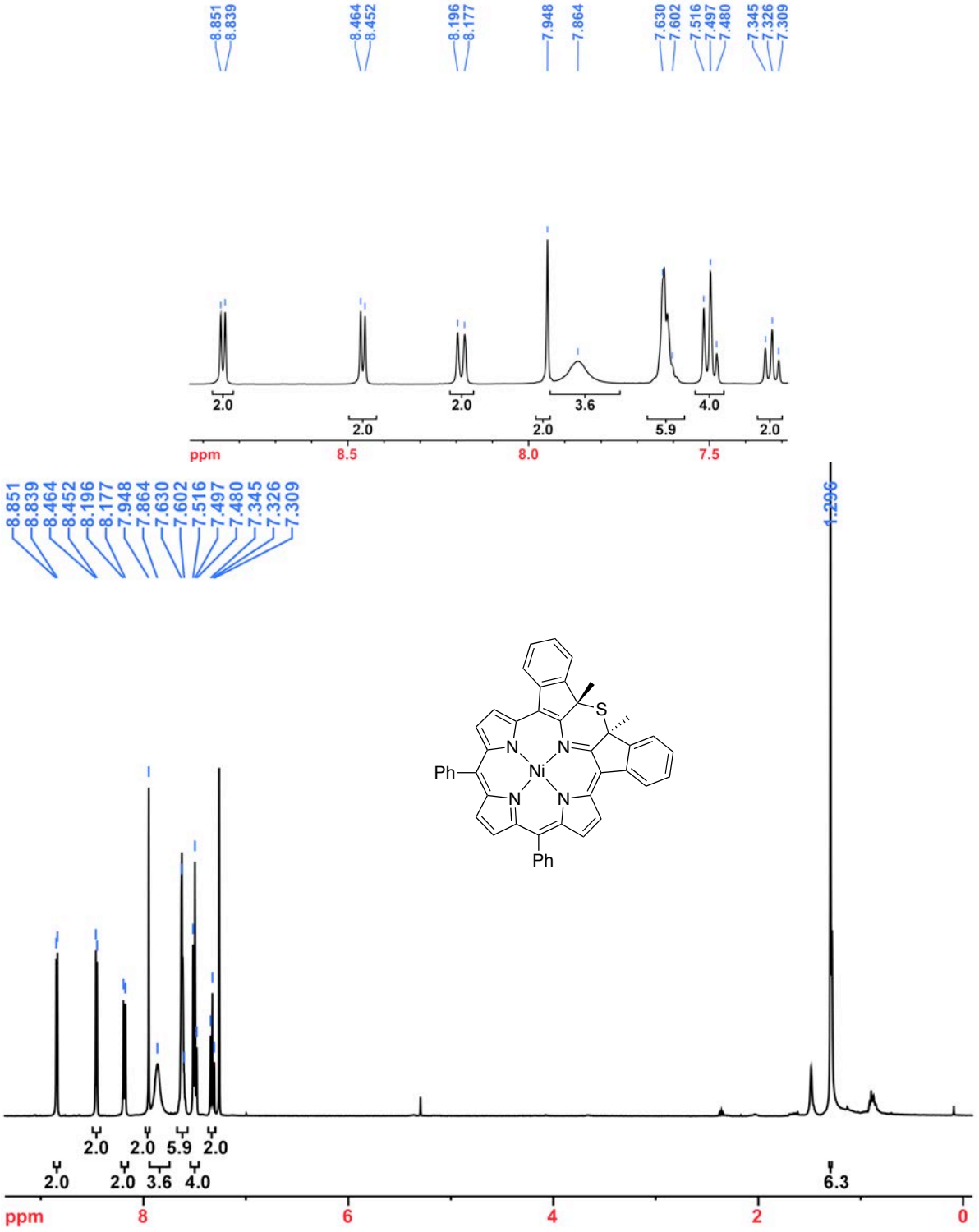

Figure S5. ^{1}H NMR spectrum (400 MHz, $CDCl_3$, 320 K) of **10Ni**

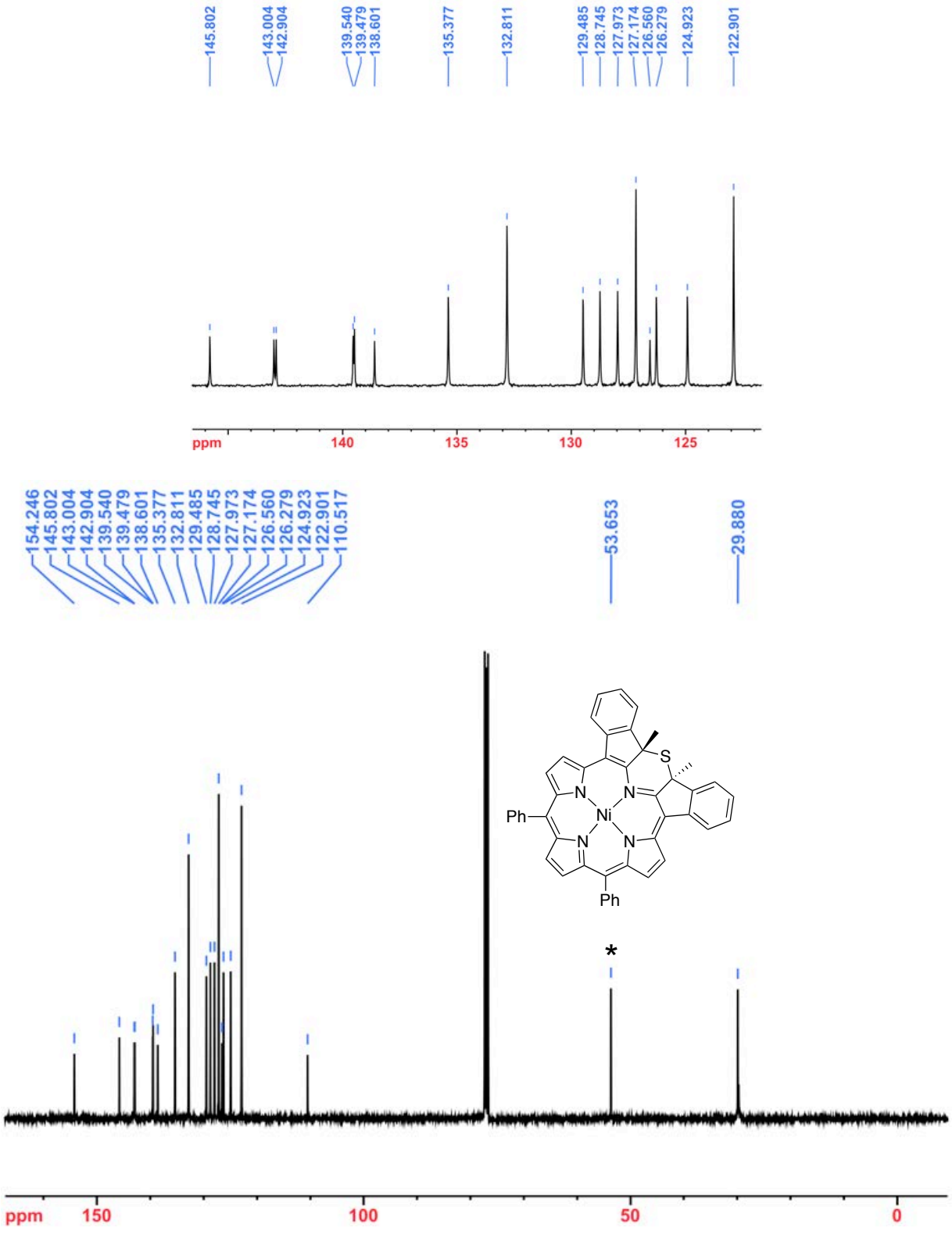

Figure S6. ^{13}C NMR spectrum (100 MHz, $CDCl_3$, 300 K) of **10Ni** * **= solvent peak**

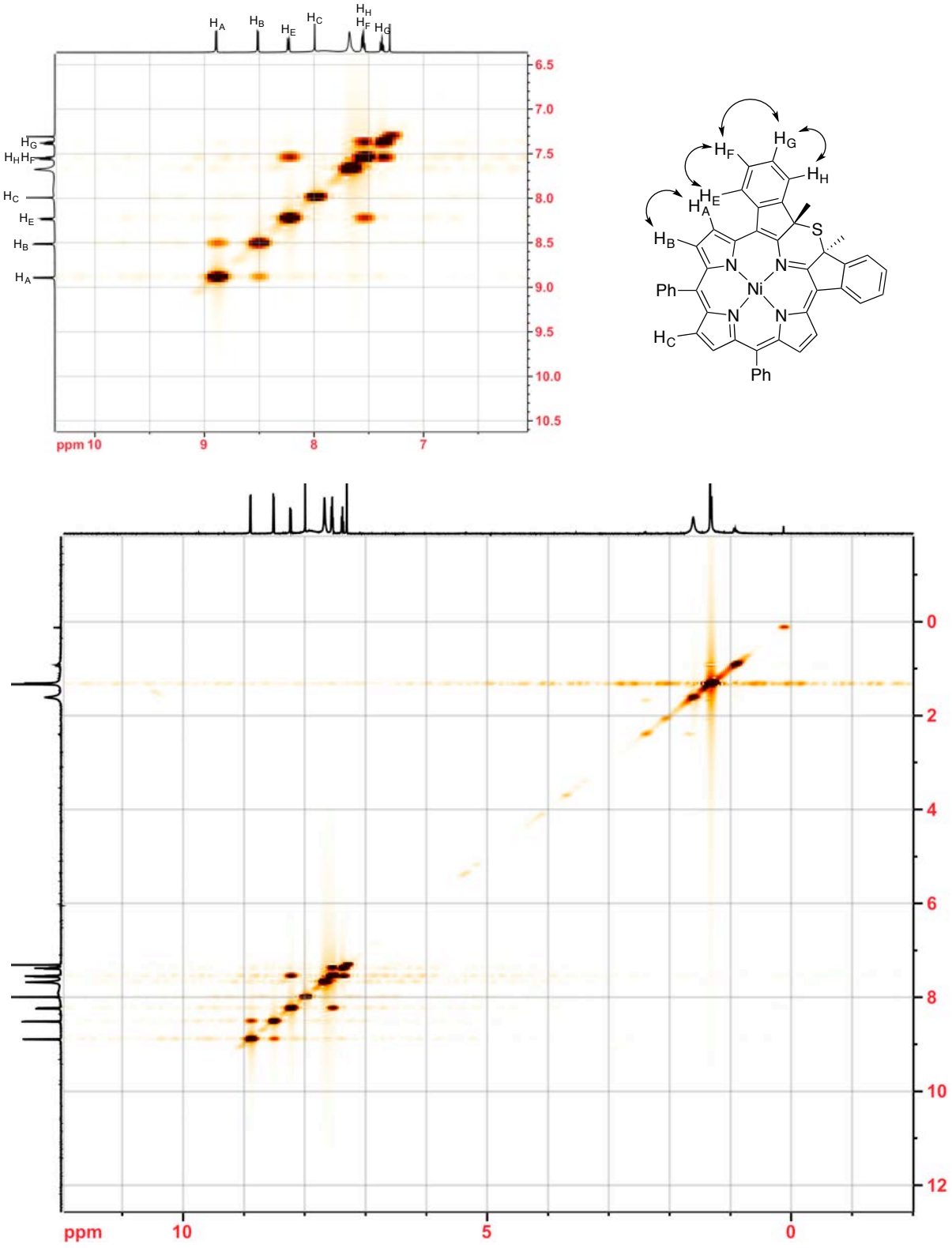

Figure S7. H,H COSY NMR spectrum (500 MHz, $CDCl_3$, 300 K) of **10Ni**

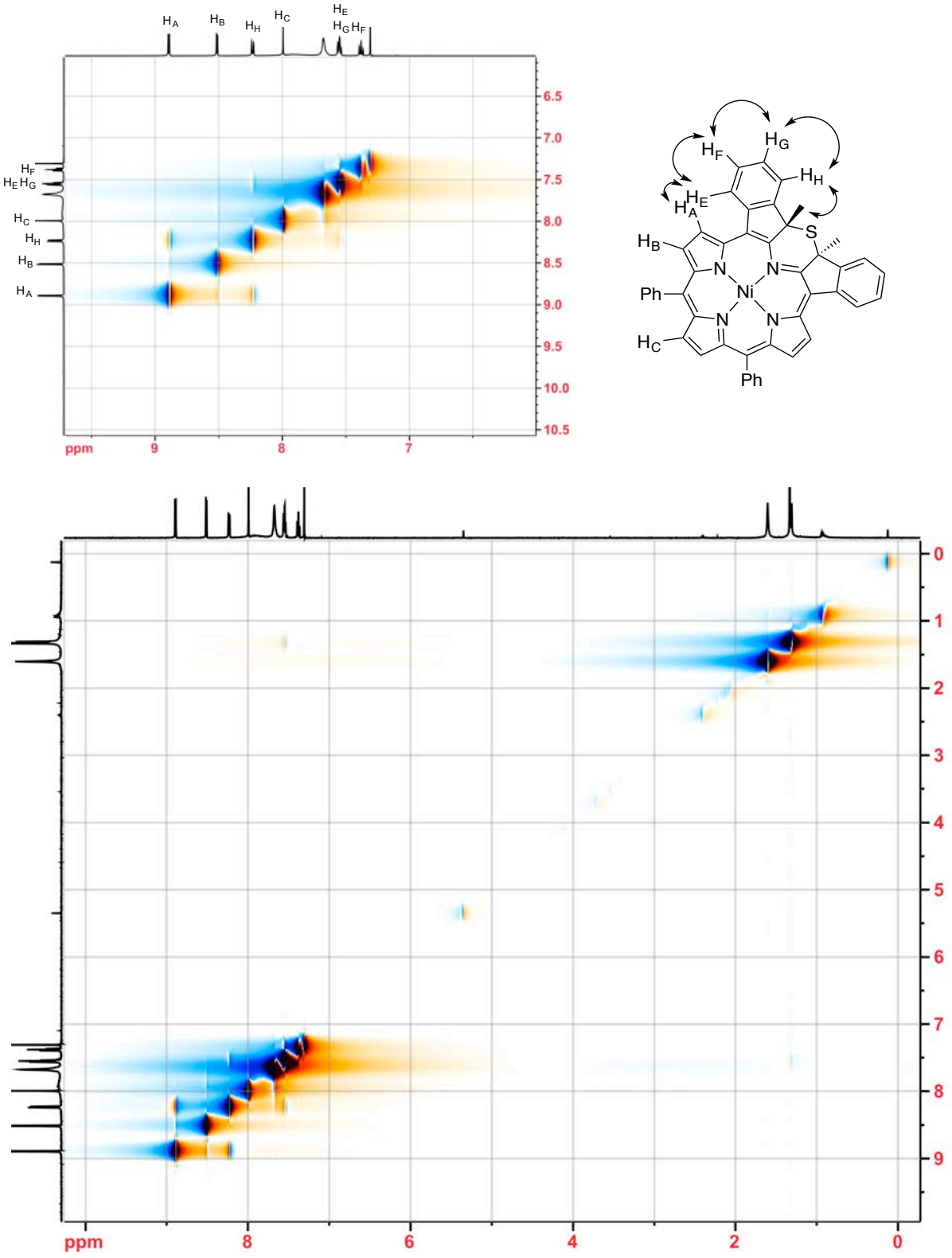

Figure S8. NOESY spectrum (500 MHz, $CDCl_3$, 300 K) of **10Ni**

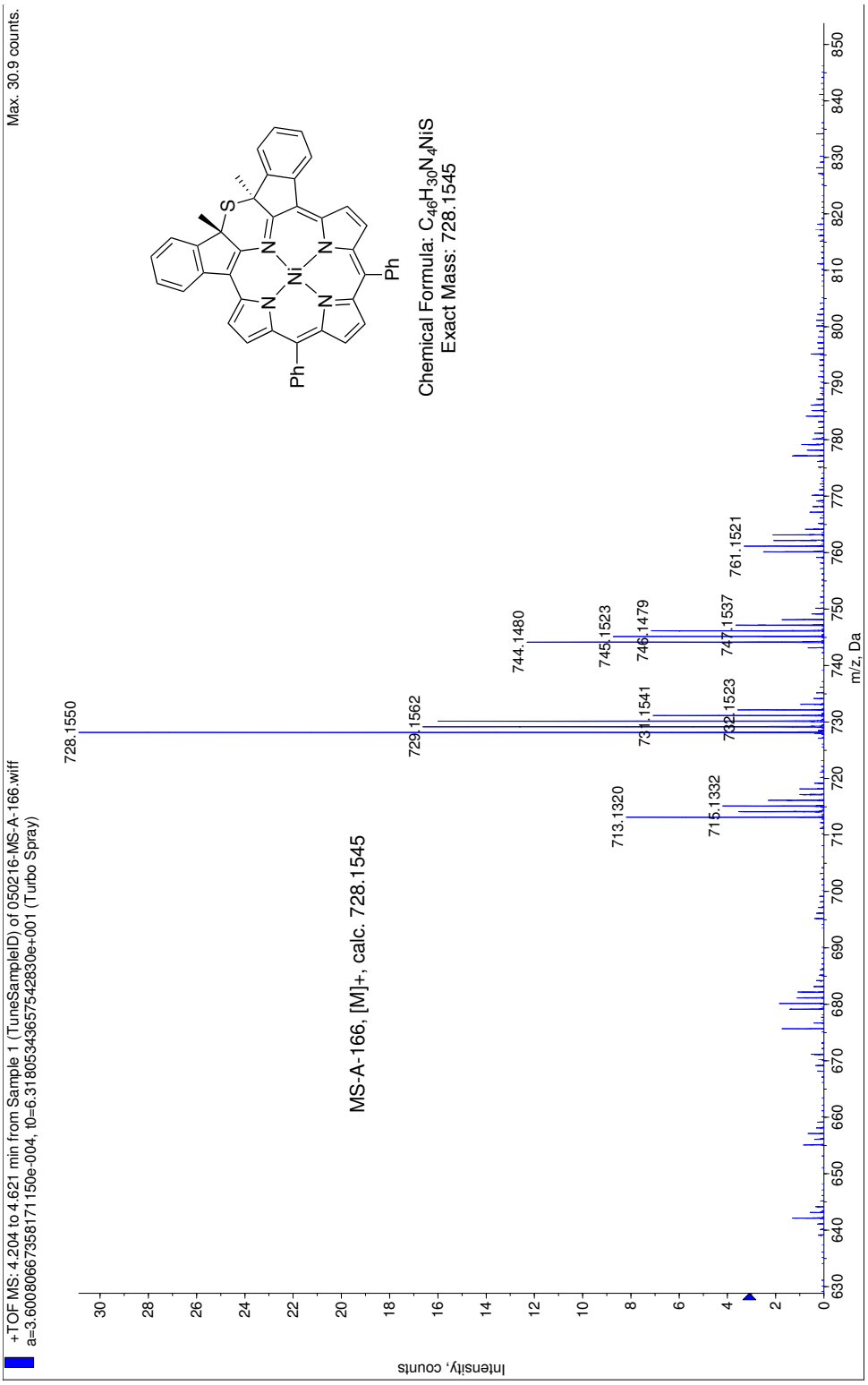

Figure S9. HR ESI+ MS (100% CH_3CN, TOF) of **10Ni**

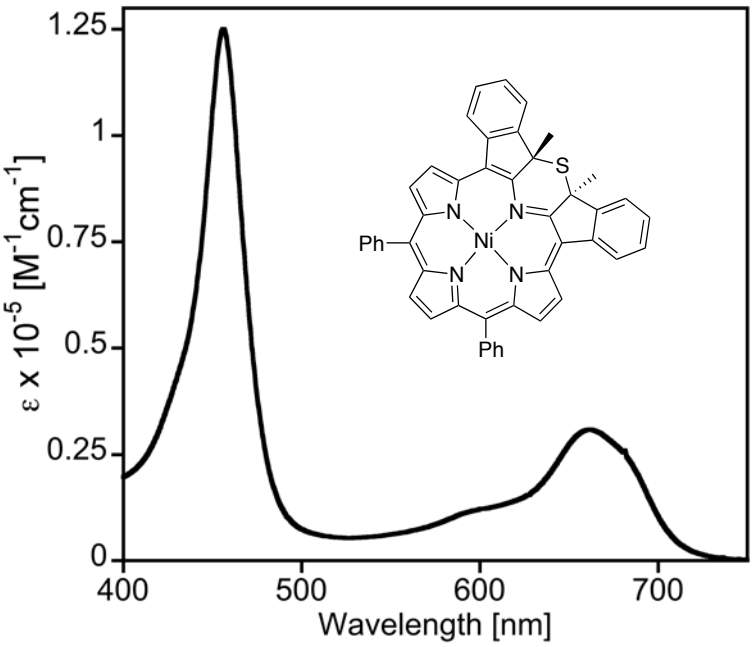

Figure S10. UV-vis spectrum (CH_2Cl_2) of 10Ni

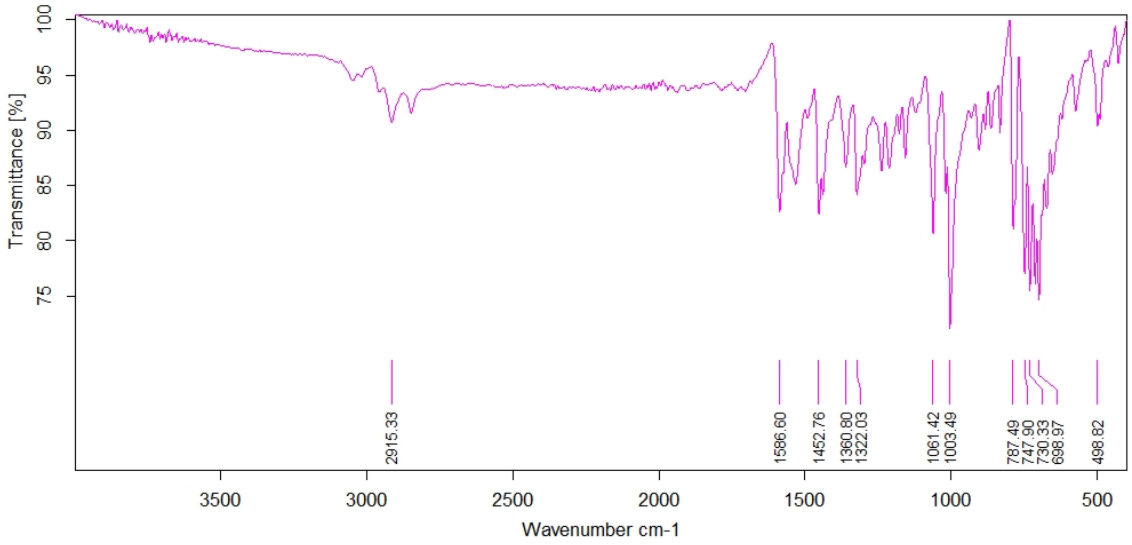

Figure S11. IR spectrum (neat, diamond ATR) of **10Ni**

Bisphenyl-linked [*meso*-Tetraphenyl-2,3-*trans*-dimethylchlorinato]Ni(II) (11Ni)

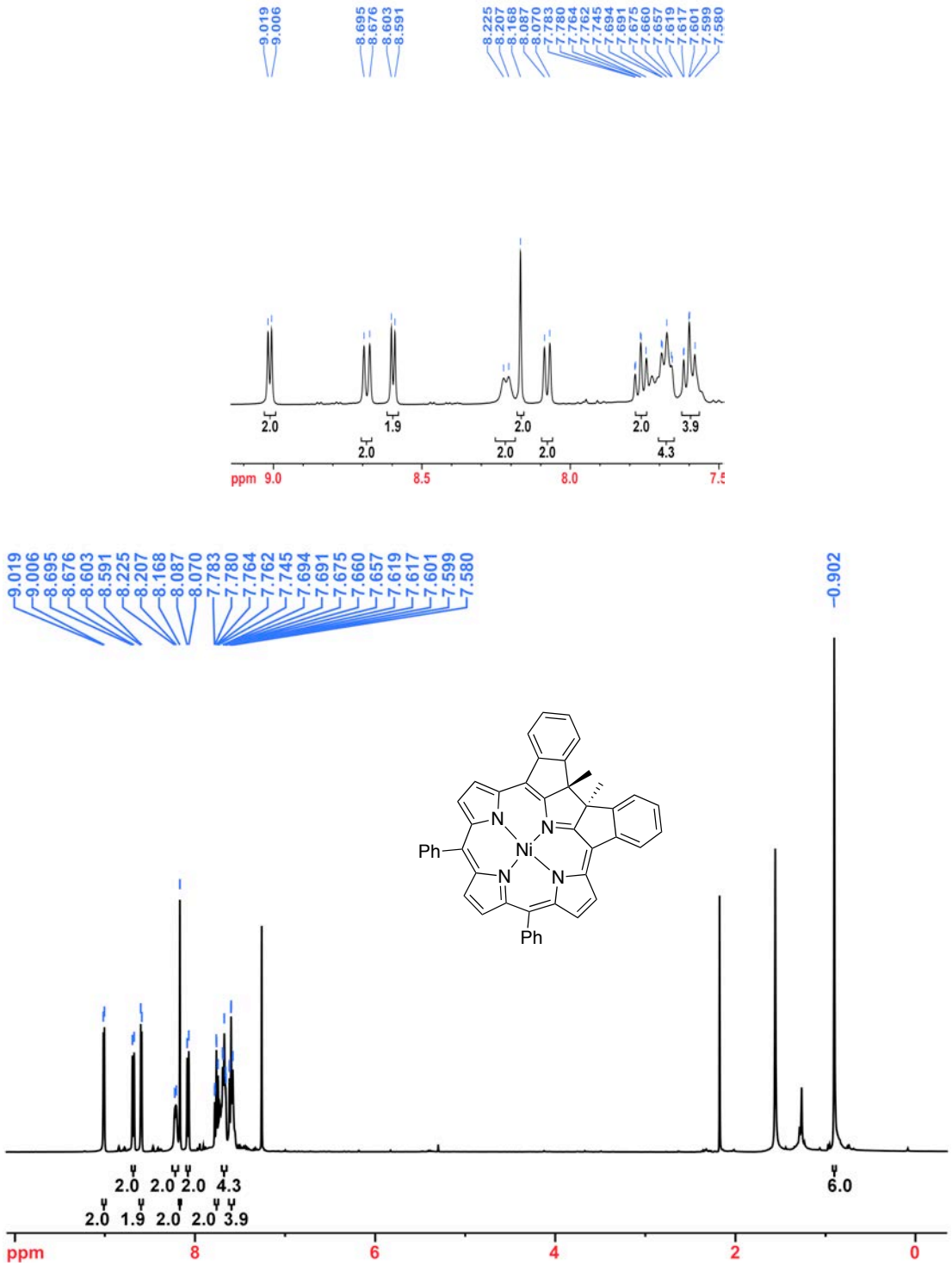

Figure S12. ^{1}H NMR spectrum (400 MHz, $CDCl_3$, 300 K) of **11Ni**

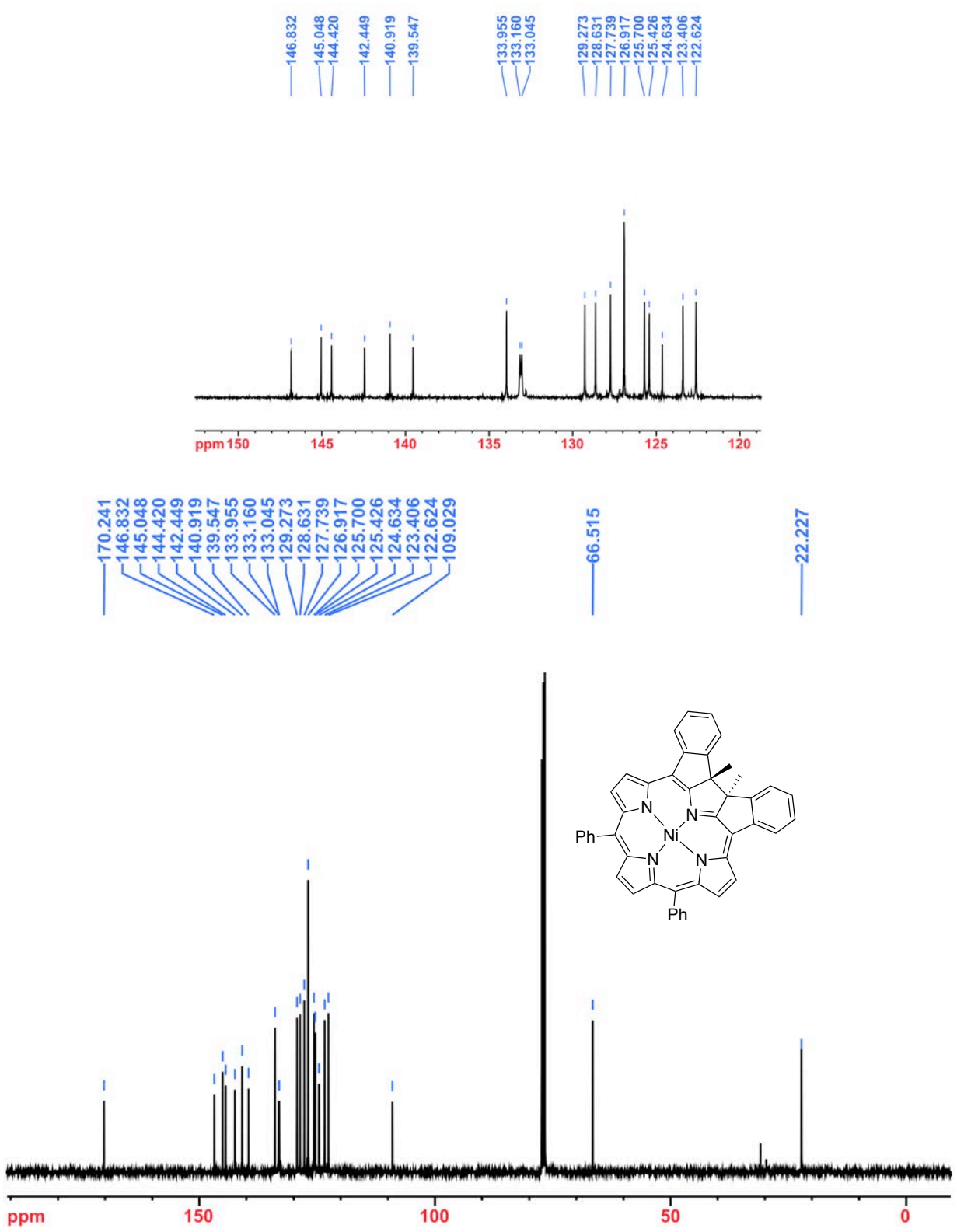

Figure S13. ^{13}C NMR spectrum (100 MHz, $CDCl_3$, 300 K) of **11Ni**

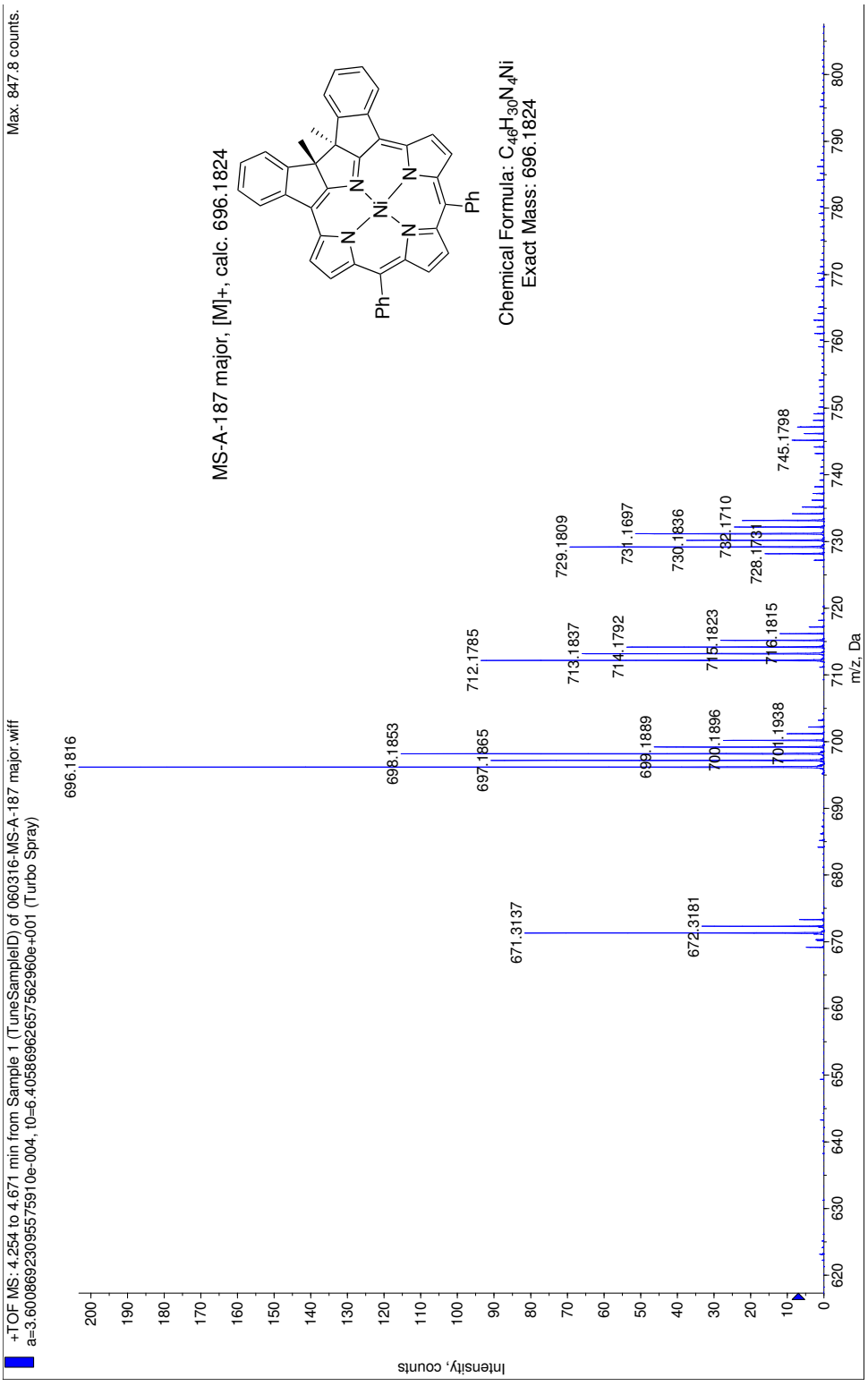

Figure S14. HR ESI+ MS (100% CH_3CN, TOF) of **11Ni**

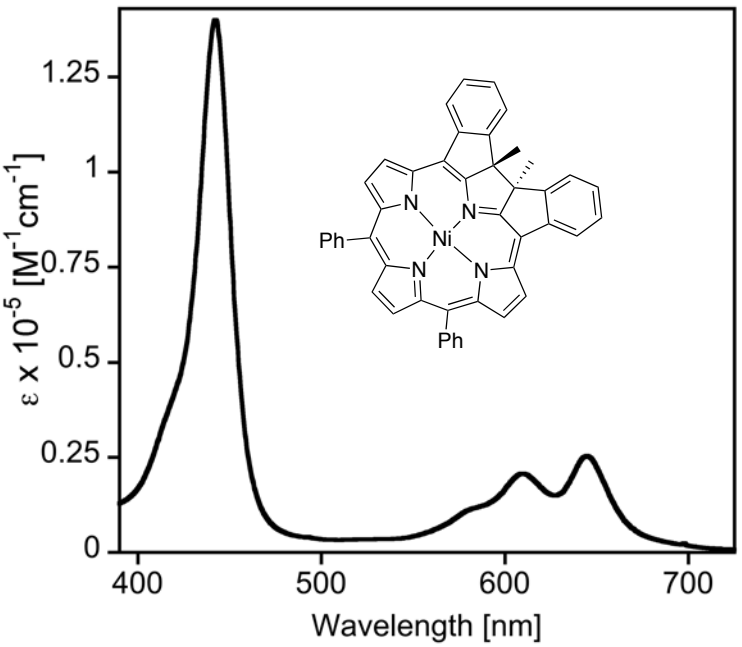

Figure S15. UV-vis spectrum (CH_2Cl_2) of **11Ni**

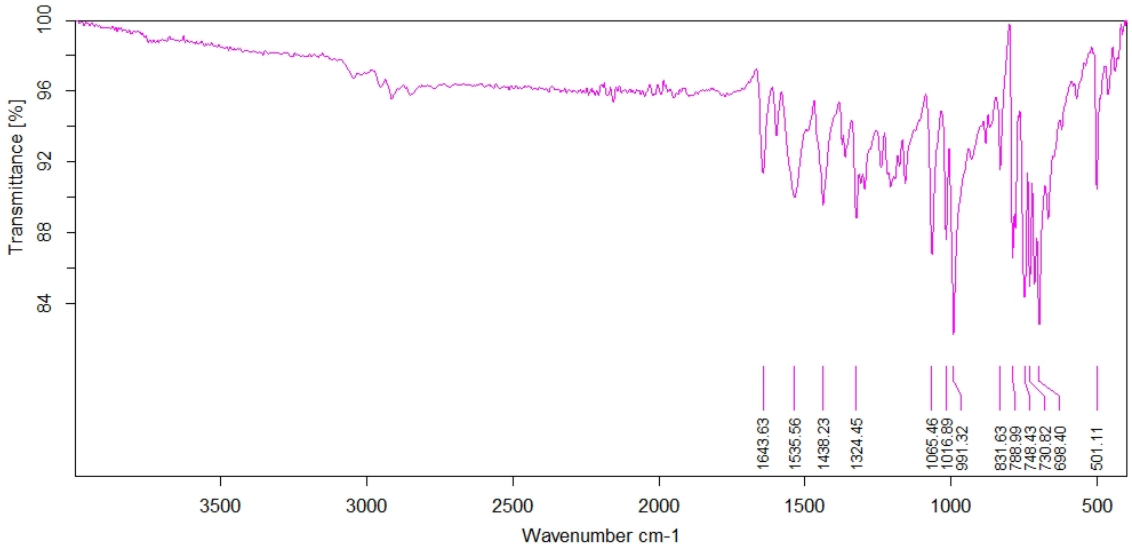

Figure S16. IR spectrum (neat, diamond ATR) of **11Ni**

Bisphenyl-linked [*meso*-Tetraphenyl-2,3-dimethylindenophyrinato]Ni(II) (12Ni)

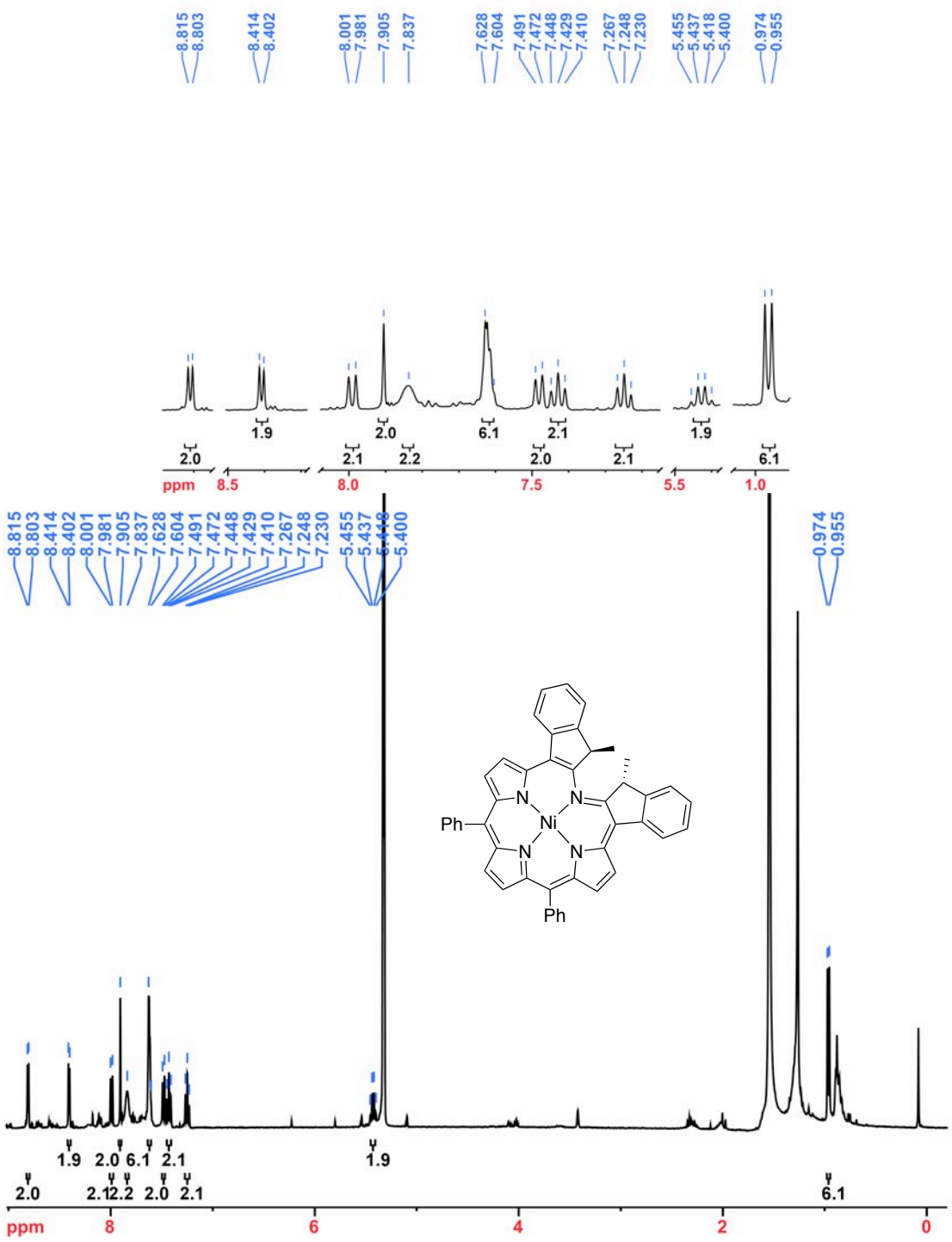

Figure S17. ^{1}H NMR spectrum (400 MHz, $CDCl_3$, 300 K) of **12Ni**

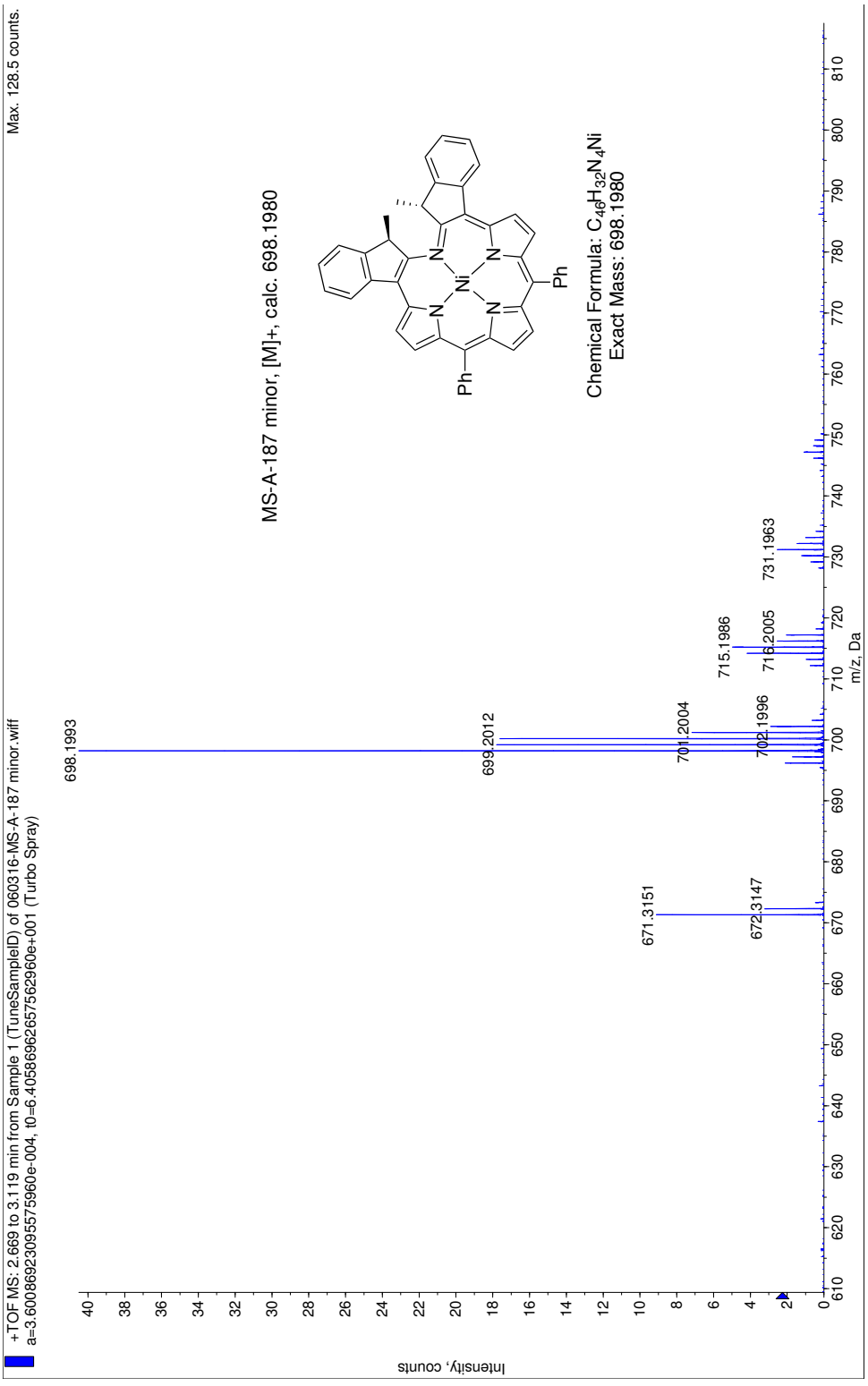

Figure S18. HR ESI+ MS (100% CH_3CN, TOF) of **12Ni**

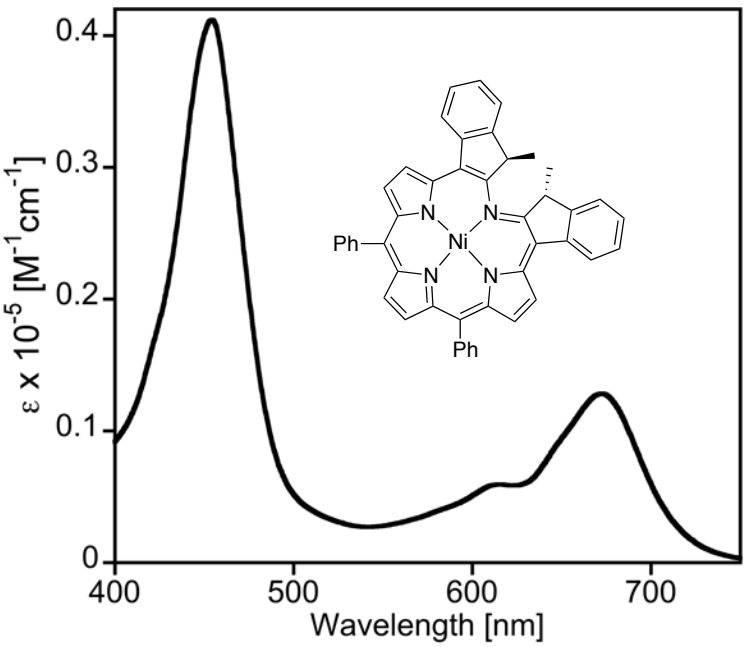

Figure S19. UV-vis spectrum (CH_2Cl_2) of **12Ni**

[*meso*-Tetraphenyl-2,3-*trans*-dimethyl-2a-oxa-2a-homoporphyrinato]Ni(II) (14Ni)

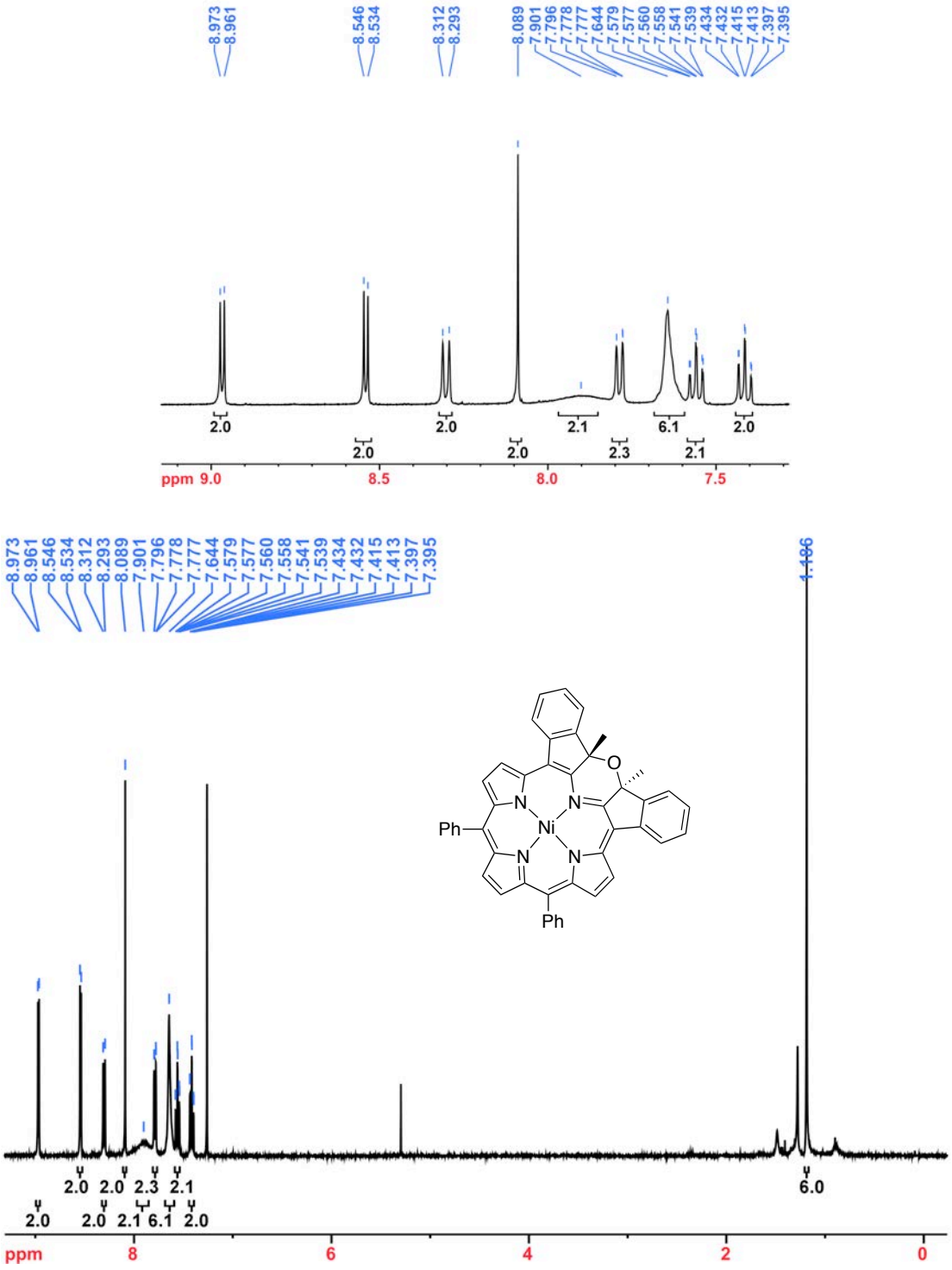

Figure S20. ^{1}H NMR spectrum (400 MHz, $CDCl_3$, 300 K) of **14Ni**

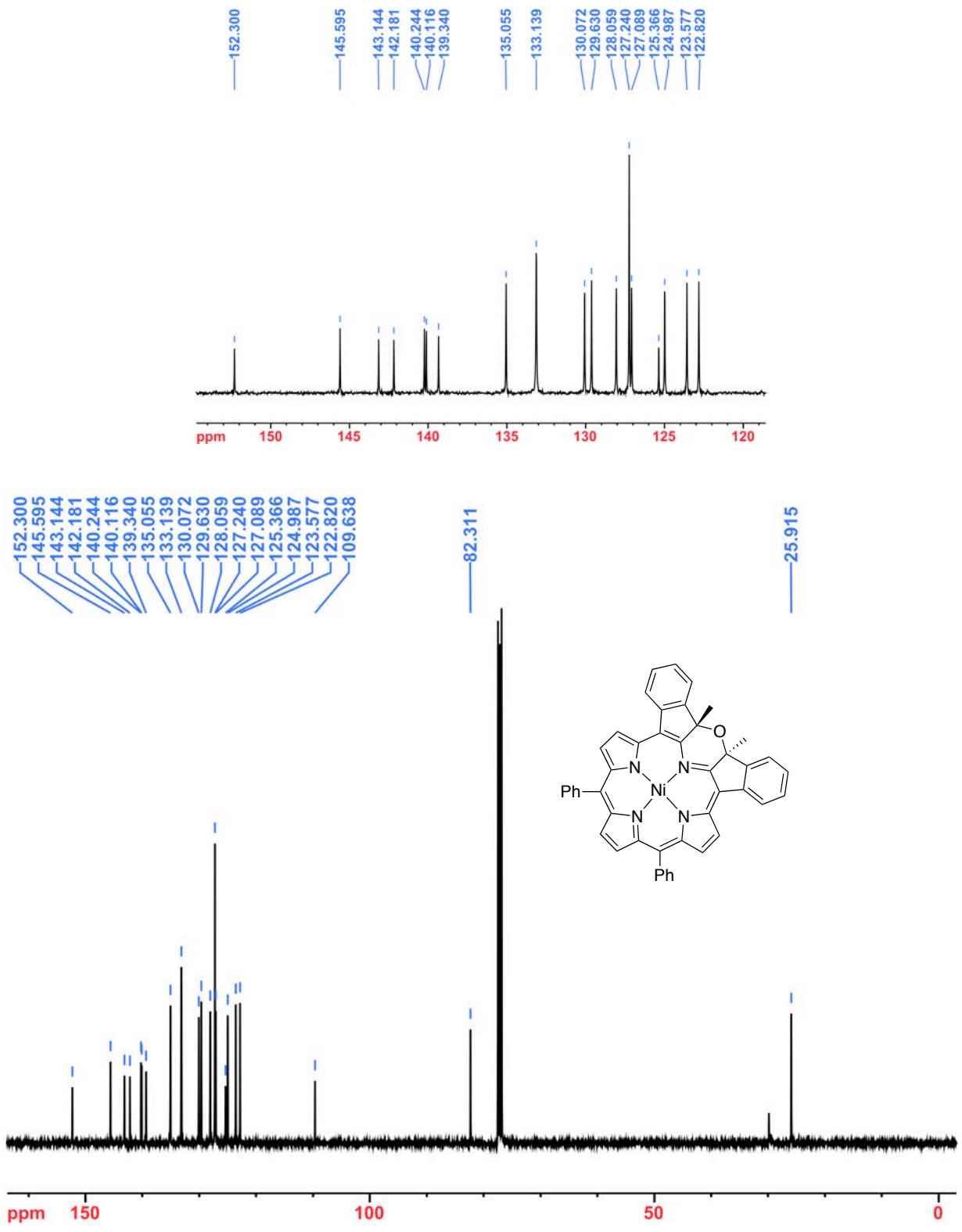

Figure S21. ^{13}C NMR spectrum (100 MHz, $CDCl_3$, 300 K) of **14Ni**

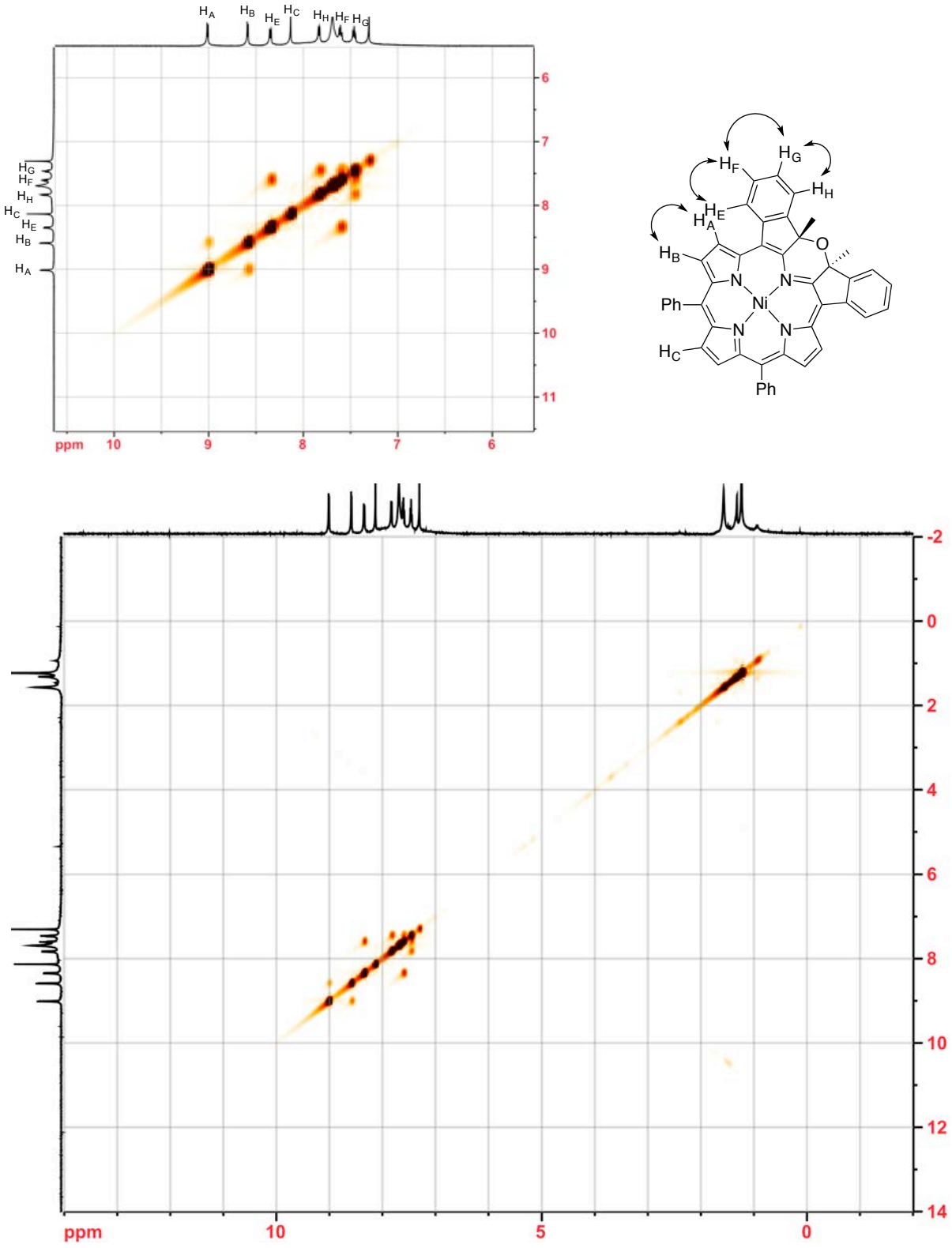

Figure S22. H,H COSY spectrum (500 MHz, $CDCl_3$, 300 K) of **14Ni**

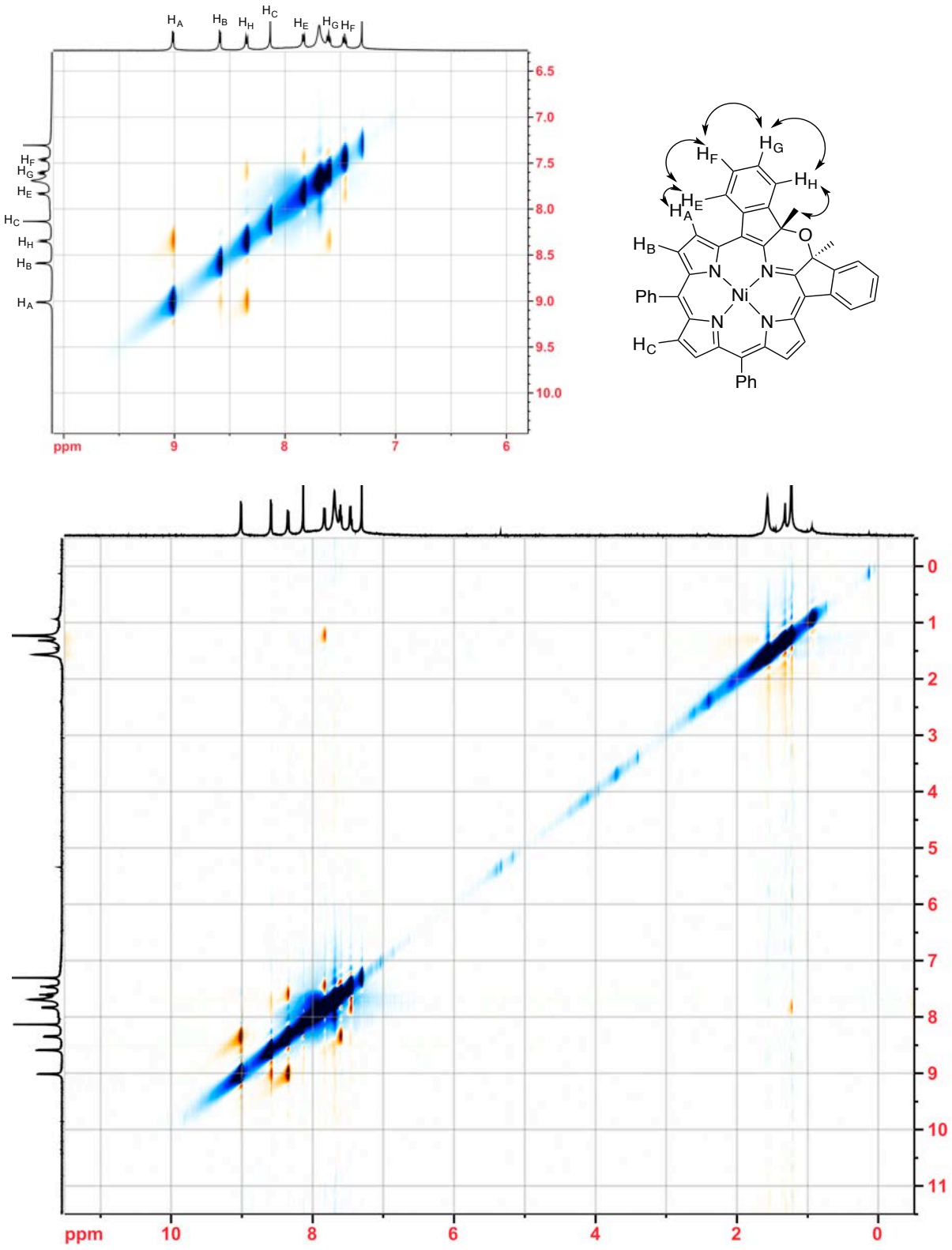

Figure S23. NOESY spectrum (500 MHz, $CDCl_3$, 300 K) of **14Ni**

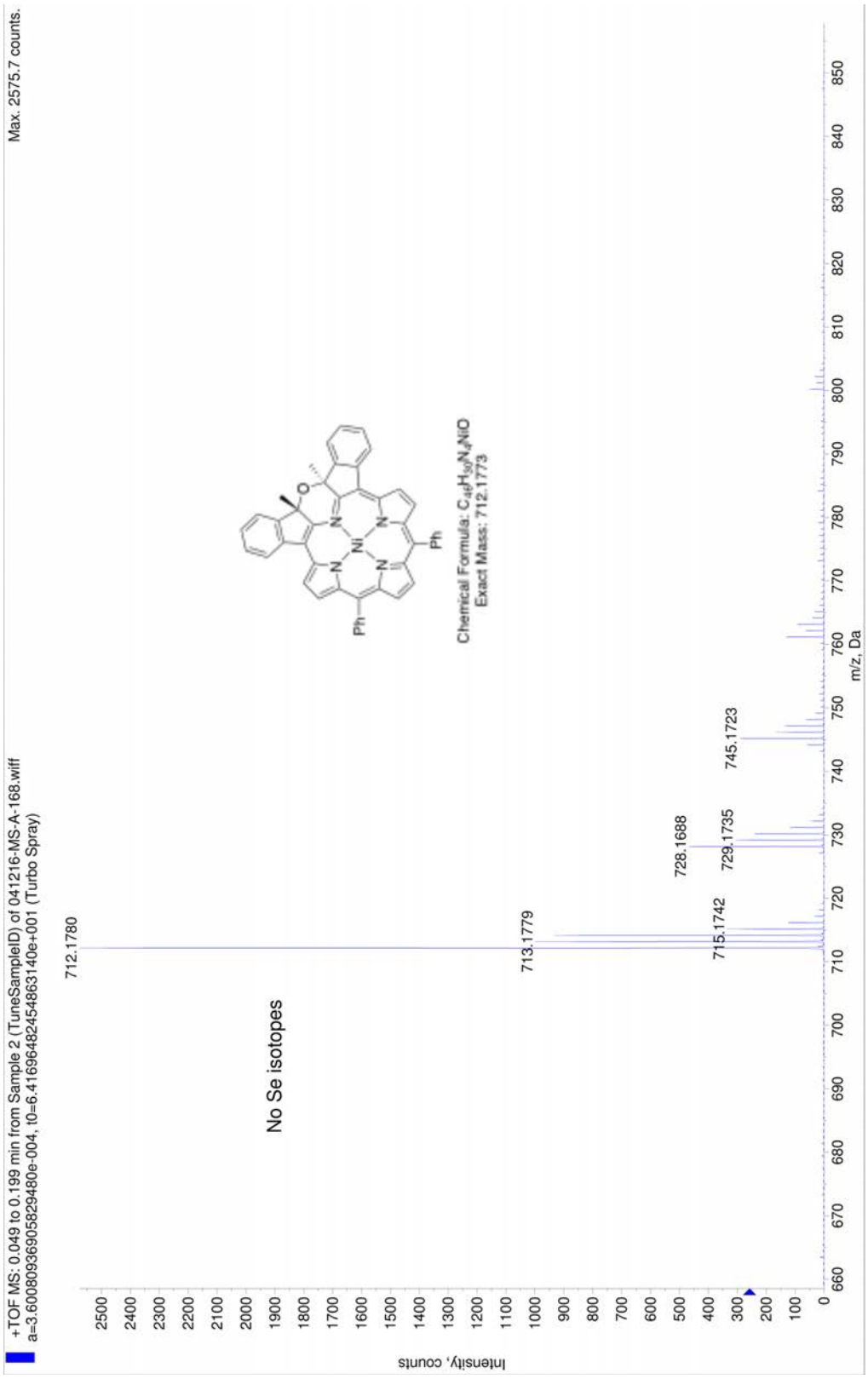

Figure S24. HR ESI+ MS (100% CH_3CN, TOF) of **14Ni**

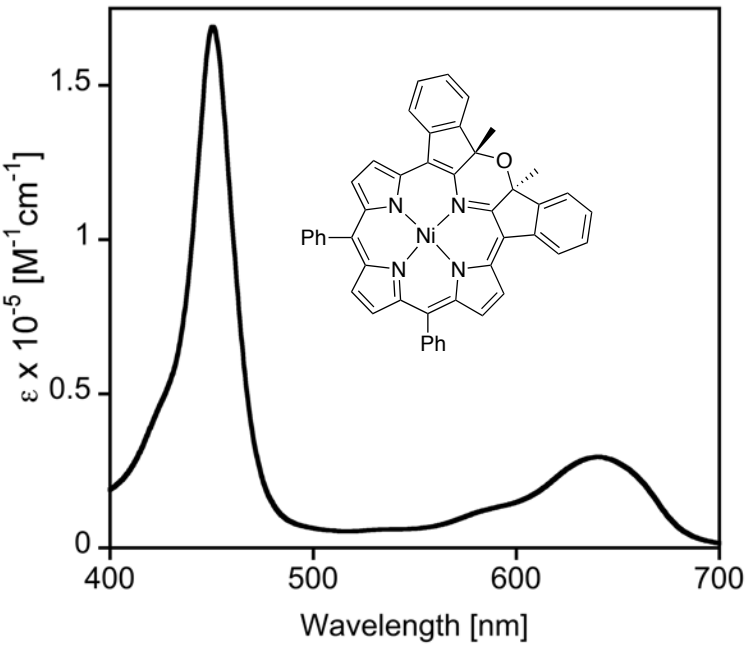

Figure S25. UV-vis spectrum (CH_2Cl_2) of **14Ni**

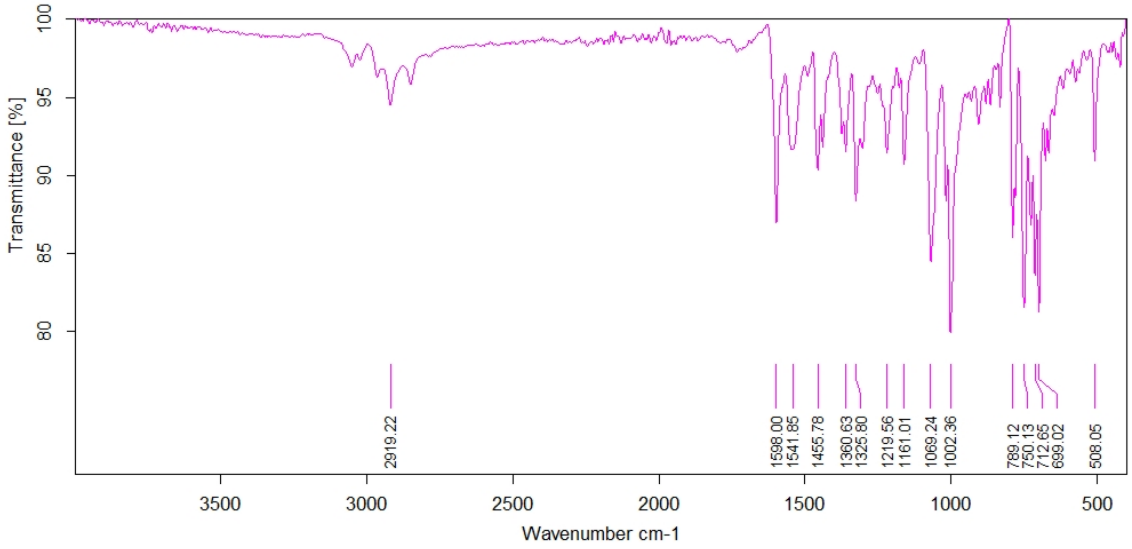

Figure S26. IR spectrum (neat, diamond ATR) of **14Ni**

Details to the X-Ray Crystal Structure Determinations

Single crystals suitable for X-ray diffraction were mounted on Mitegen micromesh mounts with the help of a trace of mineral oil. Data were collected on a Rigaku R-axis curved image plate diffractometer equipped with a MicroMax002+ high-intensity copper X-ray source with confocal optics and examined with Cu Kα radiation (λ = 1.54184 Å). Data were collected using the dtrek option of CrystalClear [1]. All data sets were processed using HKL3000, [2] and were corrected for absorption and scaled using Scalepack. [2] The space groups were assigned using XPREP from the Shexltl suite of programs [3] and the structures were solved by direct methods with SHELXS [4] and refined by full matrix least squares against F^2 with all reflections using SHELXL-2014 [5] using the graphical user interface ShelXle. [6] H atoms attached to carbon atoms were positioned geometrically and constrained to ride on their parent atoms, with carbon hydrogen bond distances of 0.95 Å for alkene and aromatic C-H, and 0.99 and 0.98 Å for aliphatic CH_2 and CH_3 moieties, respectively. Methyl H atoms were allowed to rotate but not to tip to best fit the experimental electron density. U_{iso}(H) values were set to a multiple of U_{eq}(C) with 1.5 for CH_3 and 1.2 for C-H and CH_2 units, respectively. Complete structures in CIF format have been deposited with the Cambridge Crystallographic Database. CCDC 1506186-1506188 contain the supplementary crystallographic data for this paper. The data can be obtained free of charge from The Cambridge Crystallographic Data Centre via www.ccdc.cam.ac.uk/structures.

1. Rigaku Corp. (2014). CrystalClear, The Woodlands, Texas, USA.
2. Z. Otwinowski, W. Minor, in: *Methods Enzymol.*, (1997) pp. 307–326.
3. SHELXTL (2003) Bruker Advanced X-ray Solutions, Bruker AXS Inc., Madison, Wisconsin: USA.
4. G.M. Sheldrick, Acta Crystallogr., Sect. A 64 (2008) 112–122.
5. G.M. Sheldrick, Acta Crystallogr., Sect. C 71 (2015) 3–8.
6. C.B. Hübschle, G.M. Sheldrick, B. Dittrich, J. Appl. Crystallogr. 44 (2011) 1281–1284.

Table 1. X-Ray Diffractometry Experimental Details

	8Ni	**10Ni`**	**11Ni**
Crystal data			
Chemical formula	$C_{46}H_{30}N_4NiS \cdot 1.299(C_6H_{14})$	$C_{46}H_{30}N_4NiS \cdot CH_2Cl_2$	$C_{46}H_{30}N_4Ni$
M_r	841.43	814.43	697.45
Crystal system, space group	Trigonal, $R\bar{3}:H$	Monoclinic, $P2_1/n$	Orthorhombic, $P2_12_12_1$
Temperature (K)	100	100	100
a, *b*, *c* (Å)	41.2820 (5), 41.2820 (5), 14.1626 (2)	13.8085 (4), 19.1276 (3), 14.6014 (4)	11.6977 (5), 14.2227 (6), 39.3907 (13)
a1.6977 (°)	90, 90, 120	90, 108.452 (2), 90	90, 90, 90
V (Å^3)	20902.3 (6)	3658.30 (16)	6553.5 (4)
Z	18	4	8
F(000)	7973.1	1680	2896
D_x (Mg m^{-3})	1.203	1.479	1.414
Radiation type	Cu *K*a	Cu *K*a	Cu *K*a
No. of reflections for cell measurement	85908	63420	66584
q range (°) for cell measurement	5.7–72.2	5.3–72.3	3.3–70.1
m (mm^{-1})	1.32	2.97	1.17
Crystal shape	Block	Block	Plate
Colour	Black	Black	Black
Crystal size (mm)	0.32 × 0.31 × 0.22	0.21 × 0.20 × 0.17	0.18 × 0.16 × 0.06
Data collection			
Diffractometer	Rigaku Rapid II curved image plate diffractometer	Rigaku Rapid II curved image plate diffractometer	Rigaku Rapid II curved image plate diffractometer
Radiation source	microfocus X-ray tube	microfocus X-ray tube	microfocus X-ray tube
Monochromator	Laterally graded multilayer (Goebel) mirror	Laterally graded multilayer (Goebel) mirror	Laterally graded multilayer (Goebel) mirror
Scan method	w scans	w scans	w scans
T_{min}, T_{max}	0.622, 0.760	0.568, 0.632	0.656, 0.933
No. of measured, independent and observed [I > 2s>I)] reflections	85908, 9054, 8763	63420, 7097, 6763	66584, 11829, 9779
R_{int}	0.051	0.048	0.120

q values (°)	q_{max} = 72.2, q_{min} = 5.7	q_{max} = 72.3, q_{min} = 5.3	q_{max} = 70.1, q_{min} = 3.3
(sin qsls$_{max}$ (Å^{-1})	0.618	0.618	0.610
Range of *h*, *k*, *l*	*h* = -49®= -4*k* = -50®= -5*l* = -17®=	*h* = -16®= -1*k* = -23®= -2*l* = -17®=	*h* = -14®= -1*k* = -16®= -1*l* = -48®=
Refinement			
Refinement on	F^2	F^2	F^2
$R[F^2 > 2s>F^2)]$, $wR(F^2)$, *S*	0.062, 0.143, 1.13	0.039, 0.099, 1.05	0.093, 0.259, 1.02
No. of reflections	9054	7097	11829
No. of parameters	694	499	1286
No. of restraints	330	0	1484
H-atom treatment	H-atom parameters constrained	H-atom parameters constrained	H-atom parameters constrained
	$w = 1/[s^2(F_o^2) + (0.0243P)^2 + 161.1053P]$ where $P = (F_o^2 + 2F_c^2)/3$	$w = 1/[s^2(F_o^2) + (0.0344P)^2 + 5.041P]$ where $P = (F_o^2 + 2F_c^2)/3$	$w = 1/[s^2(F_o^2) + (0.1974P)^2 + 5.651P]$ where $P = (F_o^2 + 2F_c^2)/3$
(D/32$_{max}$	0.001	< 0.001	0.003
Dρ_{max}, Dρ_{min} (e Å^{-3})	0.92, -0.79	1.05, -0.89	3.50, -0.78
Extinction method	*SHELXL2014*/7 (Sheldrick 2014, Fc*= kFc[1+0.001 x Fc^{2}l^3/sin(2qsi$^{-1/4}$	*SHELXL2014*/7 (Sheldrick 2014, Fc*= kFc[1+0.001 x Fc^{2}l^3/sin(2qsi$^{-1/4}$	None
Extinction coefficient	0.000039 (4)	0.00060 (6)	–
Absolute structure	–	–	Refined as an inversion twin.
Absolute structure parameter	–	–	0.28 (6)
CCDC #	1506186	1506187	1506188

Computer programs: *CrystalClear*-SM Expert 2.1 b32 (Rigaku, 2014), *HKL-3000* (Otwinowski & Minor, 1997), *SHELXS97* (Sheldrick, 2008), *SHELXL2014*/7 (Sheldrick, 2014), SHELXLE Rev794 (Hübschle *et al.*, 2011).

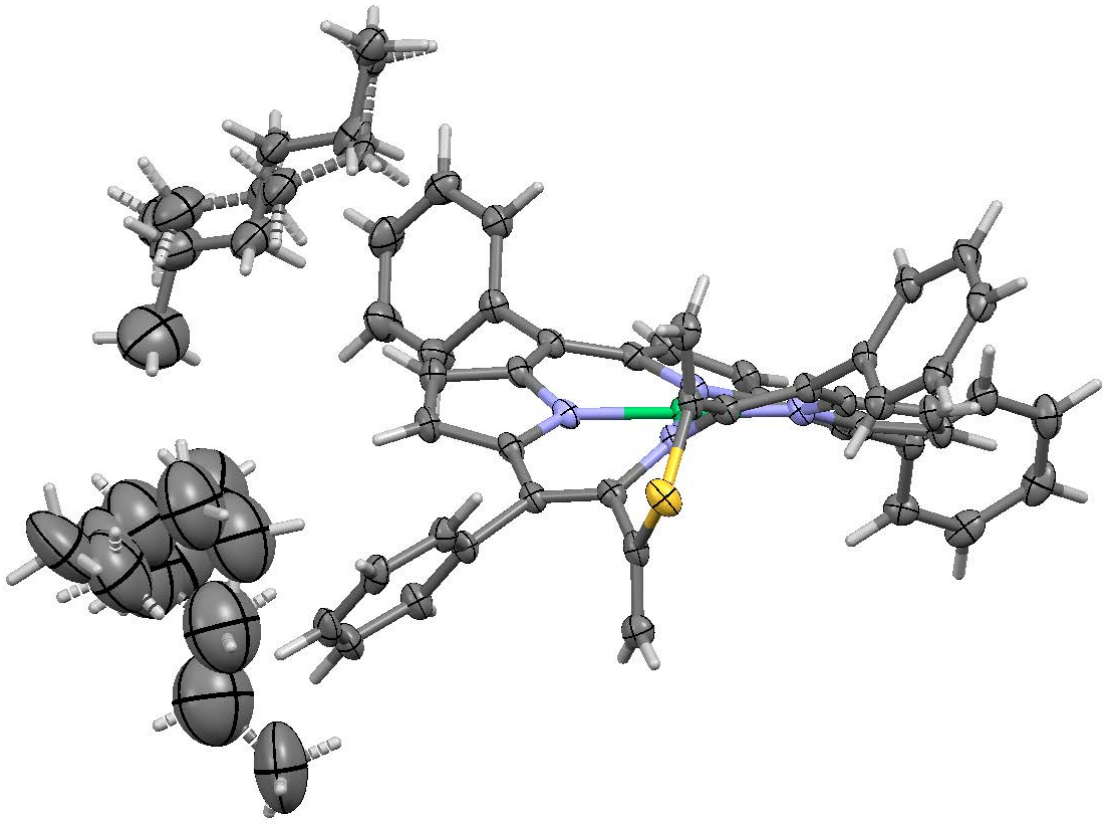

Figure S27. ORTEP style representation of **8Ni** showing disordered hexane molecules. Thermal ellipsoid probability at 50%. All labels omitted for clarity.

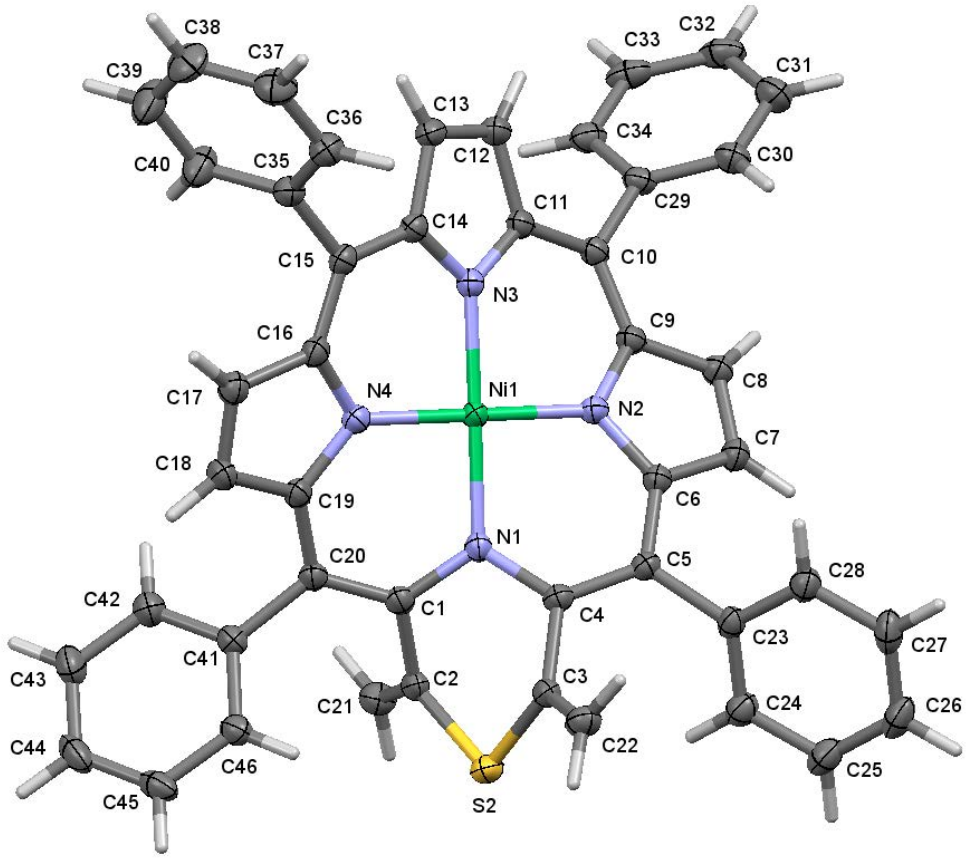

Figure S28. ORTEP style representation of **8Ni** with atom labels. Thermal ellipsoid probability at 50%. Solvate molecules and hydrogen labels omitted for clarity.

Solvate hexane molecules are disordered. One well defined but only partially occupied hexane molecule was refined as disordered over two slightly differing orientations. A channel around the three-fold axis is occupied by ill-defined solvate molecules. The site was modeled using two independent partially occupied hexane moieties. All hexane moieties were restrained to have similar geometries, and U_{ij} components of ADPs of disordered atoms were restrained to be similar if closer to each other than 1.7 Å. Subject to these conditions the occupancy rates for the first site refined to 0.575(7) and 0.153(6), that for the second site to 0.366(9) and 0.205(8).

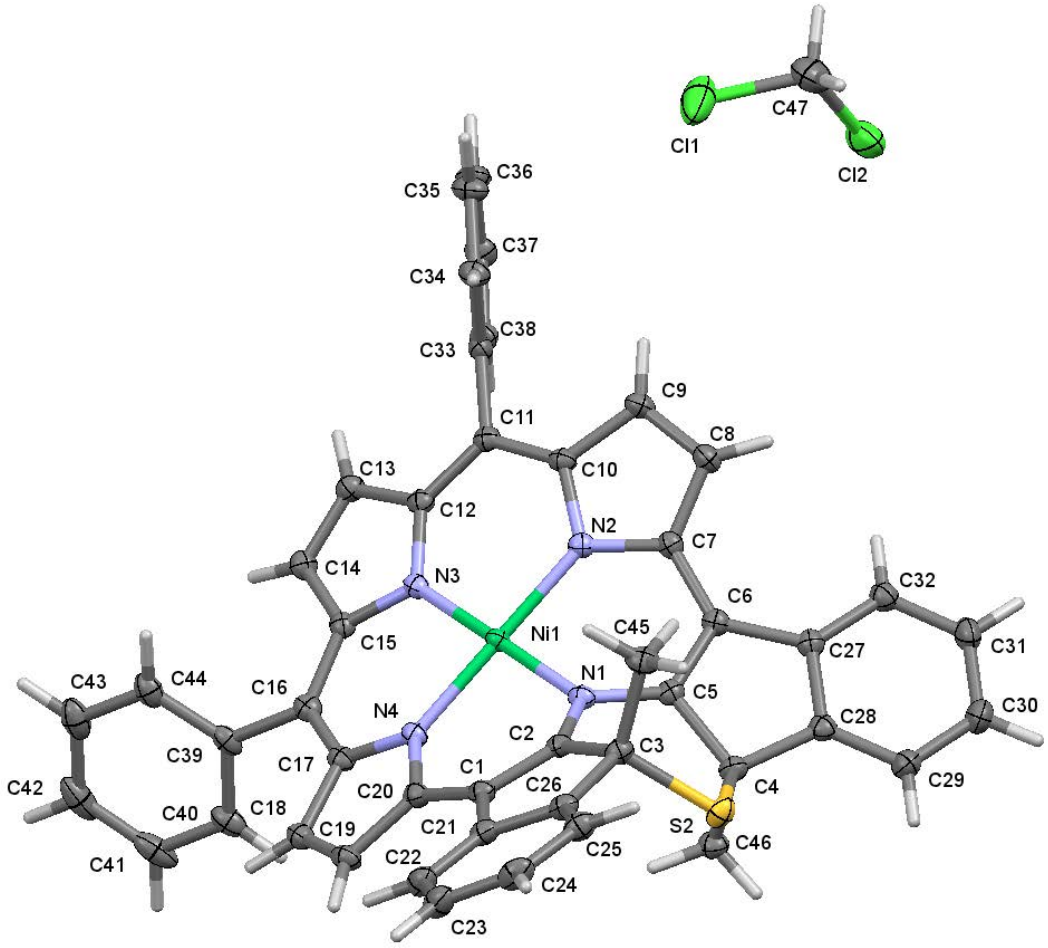

Figure S1. ORTEP style representation of **10Ni** with atom labels. Thermal ellipsoid probability at 50%. Hydrogen labels omitted for clarity.

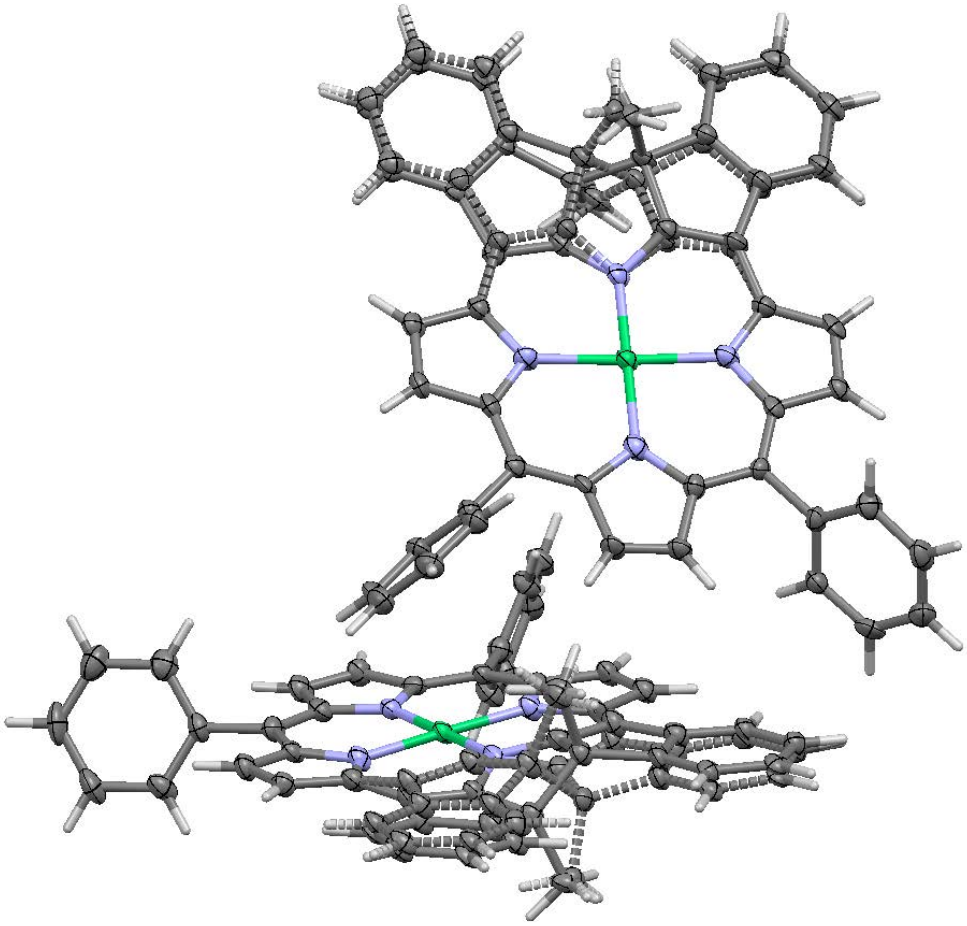

Figure S29. ORTEP style representation of **11Ni** showing disorder and both crystallographically independent molecules. Thermal ellipsoid probability at 50%. All labels omitted for clarity.

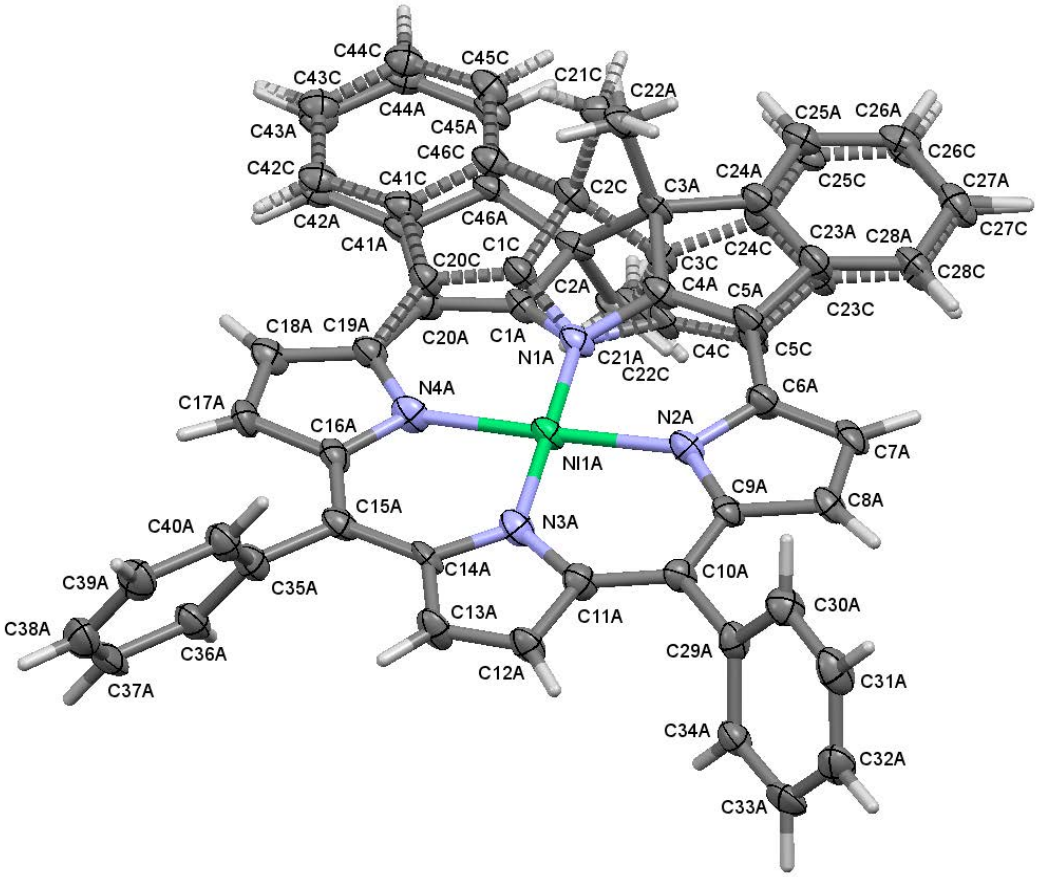

Figure S30. ORTEP style representation of first molecule of **11Ni** with labels showing disorder. Thermal ellipsoid probability at 50%. Hydrogen labels omitted for clarity.

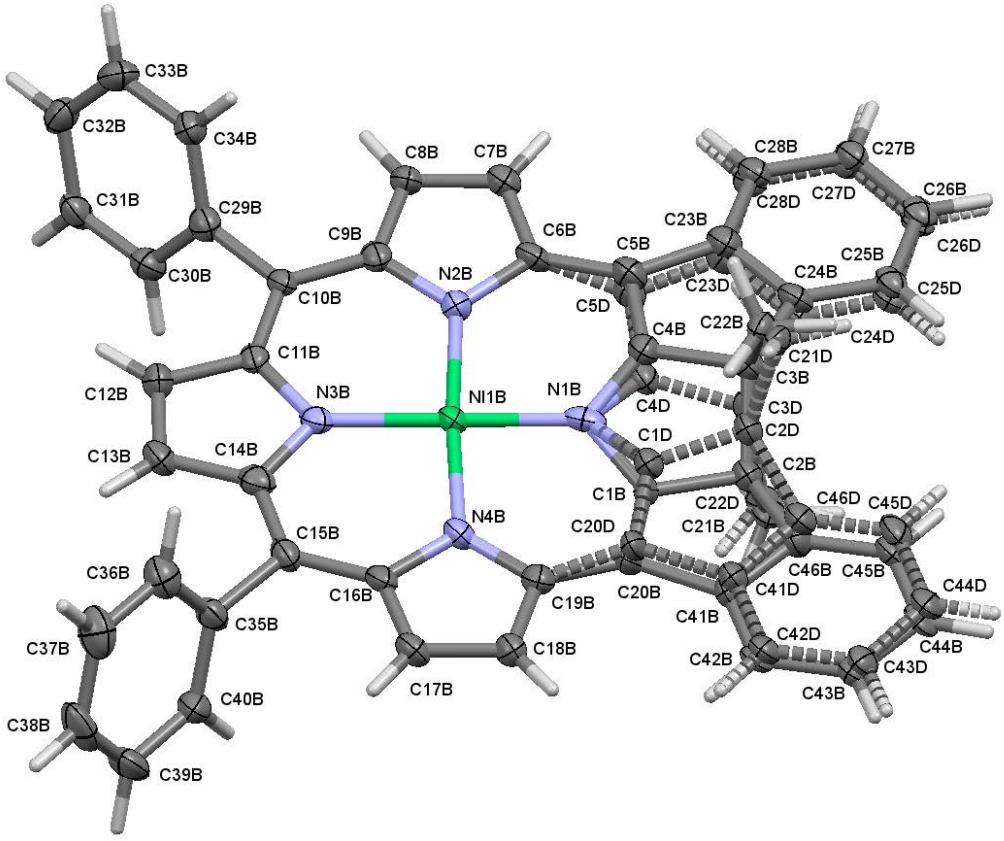

Figure S31. ORTEP style representation of second molecule of **11Ni** with labels showing disorder. Thermal ellipsoid probability at 50%. Hydrogen labels omitted for clarity.

Pronounced non-Bragg behavior was observed for the crystals tested with smeared out non-Bragg diffraction intensity between spots along the long unit cell axis.

Disorder is observed by pseudo-rotation around an axis formed by the metal ion and the center of the C2-C3 bond. The major and minor moieties of the disordered sections were restrained to have similar geometries, and selected sections of the minor moieties were restrained to be close to planar. U_{ij} components of ADPs of disordered atoms were restrained to be similar for atoms closer than 1.7 Å. Subject to these conditions occupancy ratios refined to 0.745(11) to 0.255(11) and 0.736(11) to 0.264(11).